Coherent control using adaptive learning algorithms

B. J. Pearson, J. L. White, T. C. Weinacht, and P. H. Bucksbaum
Physics Department, University of Michigan, Ann Arbor, Michigan 48109-1120
(Received 14 August 2000; published 16 May 2001)

We have constructed an automated learning apparatus to control quantum systems. By directing intense shaped ultrafast laser pulses into a variety of samples and using a measurement of the system as a feedback signal, we are able to reshape the laser pulses to direct the system into a desired state. The feedback signal is the input to an adaptive learning algorithm. This algorithm programs a computer-controlled, acousto-optic modulator pulse shaper. The learning algorithm generates new shaped laser pulses based on the success of previous pulses in achieving a predetermined goal.

DOI: 10.1103/PhysRevA.63.063412 PACS number(s): 32.80.Qk, 42.50.Hz, 33.80.−b

I. INTRODUCTION

An original impetus for coherent control was mode-selective laser photochemistry. This dream of exciting a specific bond with a laser has dimmed for various reasons. Control is hampered by fast relaxation, complicated mode structure, imperfect knowledge of the inter-nuclear potentials along arbitrary coordinates, and the distorting influence of the strong external light fields. Recent theoretical [1] and experimental advances have led to successful control of molecular ionization and dissociation [2,3], atomic and molecular fluorescence [4–6], and excitations or electrical currents in semiconductors [7–9]. Control has been predicted and demonstrated in several systems that have only two interfering pathways [2,8,9].

Strongly coupled systems such as large molecules in condensed phase are so complicated that it is nearly impossible to calculate optimal pulse shapes in advance. Recent efforts have used experimental feedback as suggested by Judson and Rabitz [1] to determine the optimal optical pulse shape to achieve a particular control goal [3,5]. In the absence of detailed knowledge of the system Hamiltonian, an algorithm must be used for selecting new pulse shapes inside the feedback loop.

This paper presents a detailed investigation of a learning strategy incorporating a modified genetic algorithm (GA) [10] in order to discover control pathways in complicated physical systems. Experiments have been carried out in a variety of molecular systems whose common feature is the existence of observable physical properties that depended on the incident (shaped) light. Several systems are described. In the gas phase, we explore nonlinear control of ionization channels in diatomic sodium. Several liquid phase experiments are also described, including control of self-phase modulation in CCl_4 and excitation of vibrational modes in methanol and benzene.

In addition to traditional GA search strategies, we incorporate other search methods that all run concurrently. The algorithm adapts itself during a run in order to search the phase space most efficiently. Because of this, it is possible to obtain physical insight into the problem under investigation, not only through the pulse-shape solutions, but also by how the algorithm arrived at those solutions. We demonstrate that our adaptive evolutionary algorithm is capable of controlling a diverse array of systems.

II. EXPERIMENTAL SETUP

The control light field is made with a Kerr lens mode-locked (KLM) titanium sapphire laser that produces 100 fs pulses with about 5 nJ of energy at a central wavelength of 790 nm (see Fig. 1). The pulses are temporally dispersed to 150 ps in a single grating expander and amplified to 2 mJ in a regenerative amplifier at 10 Hz. The output of the amplifier is split to form two beams. One beam is sent to the pulse shaper, and the other is used as an unshaped reference for spectral interferometry measurements of the shaped pulses [11]. The pulse shaper consists of a zero dispersion stretcher with an acousto-optic modulator (AOM) in the Fourier plane, where different colors in the light pulse map to different positions on the modulator [12]. The AOM carries a shaped acoustic traveling wave, which diffracts different colors with different phases and amplitudes. These colors are reassembled at the output of the pulse shaper, yielding a temporally shaped laser pulse. In order to compensate for the low efficiency of the pulse shaper (10−15%), we reamplify the shaped pulses in a low-gain multipass amplifier. The pulses are then compressed in a single grating compressor. The resulting shaped laser pulses are then directed into the molecu-

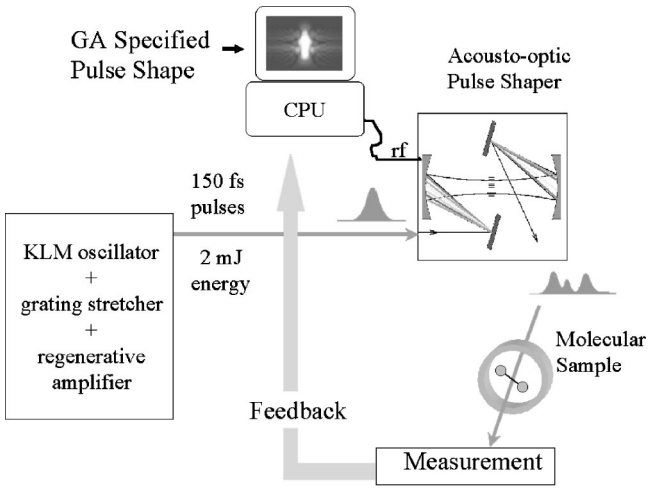

FIG. 1. Diagram of the experimental setup. The shaped laser pulses interact with a molecular sample, and a single-valued feedback function is returned to the computer. The algorithm uses these values to determine the mating procedure.

 ©2001 The American Physical Society

lar sample to be studied, and a predetermined feedback signal is monitored.

III. THE LEARNING ALGORITHM

A. Constructing the algorithm

In previous work, we demonstrated control of simple quantum systems using feedback [13]. Now we wish to control more complex systems where the optimal pulse shape is not known *a priori*. The pulse shaper has 8 bit control over the amplitude and phase of 100 different frequency components, so there are 2^{1600} different pulse shapes. The physical system couples different frequencies, so they cannot each be optimized independently. This presents a vast phase space for the search algorithm. The search must also be robust in the face of experimental noise, and capable of escaping local maxima in a rough potential energy landscape.

These requirements led us to consider a genetic algorithm, which fulfills all of these conditions: It does not rely on any local information about the search space, such as derivatives, and it is capable of handling a multidimensional phase space in the presence of noise. Previous work with adaptive feedback found genetic algorithms (or similar evolutionary strategies [14]) adept at solving similar problems [1,3,15]. A GA provides a general, robust approach to optimization, requiring little prior information about the problem to be solved. Furthermore, the GA can generate new pulse shapes that differ radically from the previous pulse shapes, to quickly sample different sections of the phase space. Our GA implementation is derived from the *Handbook of Genetic Algorithms*, a standard treatise on the subject [10].

Genetic algorithms are a class of search and optimization algorithms inspired by biological evolution. In evolution, natural selection links a string of genes to the structures that it represents. The gene string carries all of the information, while a structure's success determines its chance of reproducing. Nature knows nothing about the problem to be solved; gene strings encoding successful structures merely reproduce more often. During reproduction, the algorithm has no regard for the structure represented by the gene string. Offspring have new gene strings representing new, and possibly more successful, structures. By incorporating these ideas, a GA can solve surprisingly difficult problems. Each possible solution (structure) in the search space is given a representation (gene string). This representation is called an individual, and a group of individuals is called a population.

A basic example of a GA's implementation is shown in Fig. 2. Each individual in the population is evaluated on a given molecular sample. The individuals are ranked from most to least fit based on a predetermined single-valued feedback function (the fitness). These individuals (parents) then reproduce according to some protocol, called mating. The most fit individuals reproduce more than the least fit ones. The offspring (children) form a new population (the second generation). This reproduction and evaluation process repeats itself until terminated. The fittest current members of the population survive until the end.

In our experiments, each individual corresponds to a pulse shape, which is encoded as a string of floating point numbers

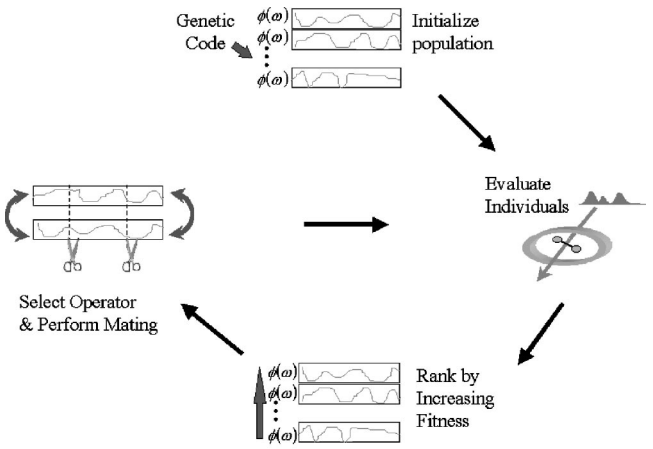

FIG. 2. The adaptive algorithm begins by initializing a random population of pulse shapes. These pulse shapes interact with the molecular system and are ranked according to fitness. These fitnesses, as well as the fitnesses of the various operators, are used to select the individuals and operators to be used in the mating. After the new generation of pulse shapes is created, the cycle repeats.

specifying the phase and amplitude at the various frequency components of the laser pulse. The algorithm typically controls the phases for 20 to 60 colors, linearly interpolating the phases for colors between the specified frequencies. Unlike the phases, which vary continuously, the amplitudes are set at discrete levels (between 3 and 40). The actual number of amplitude genes was usually less than the number of phase genes (between 10 and 20). For some of the experiments, the learning algorithm is only allowed to vary the phases of the frequency components. This fixes the energy in each pulse shape, and the algorithm simply determines how to best distribute this energy in time.

Our population normally consists of 60 individual pulse shapes. The first generation is composed of random individuals. Each pulse shape in the population interacts with the physical system under investigation and is evaluated for fitness. Our learning algorithm implements a process known as roulette wheel selection, in which an individual's chances of reproduction are proportional to its fitness, so that more fit individuals reproduce more often. In addition, a given number of the most fit parents are passed on to the next generation. This technique, known as elitism, ensures that good genetic material is not lost if by chance one of the best individuals is not chosen for reproduction or does not reproduce fruitfully.

B. Operators

The protocol for the production of new children is carried out by mathematically defined *operators* that act on the gene strings of the pulse shapes. A traditional GA uses a mixture of *crossover* and *mutation* operators, both of which are described below. We have incorporated new operators to include many different methods for searching the available phase space. The algorithm then combines the entire set of mating operators into a pool, and the various operators are allowed to compete against each other for the chance to pro-

duce new pulse shapes. This learning strategy determines which combination of methods is best for solving the particular problem.

We can categorize our operators as traditional GA operators (crossovers and mutations), or nontraditional operators. Traditional operators generate new pulse shapes from old ones on a strictly statistical basis. Traditional operators that we use include *two-point crossover*, *average crossover*, *mutation*, and *creep*. Nontraditional operators generally search the phase space by modifying the pulse shapes in a way that is guided by the physics of the system. Examples of these operators that we use include *smoothing*, *time-domain crossover*, and *polynomial phase mutation*. A well-chosen set of operators can greatly enhance the performance of the learning algorithm. Our learning algorithm is general and not limited to the operators listed above. As has been discussed elsewhere, it is possible to add other operators to the pool, even including entirely new search algorithms, such as simulated annealing [16]. If simulated annealing happens to be the method best suited to the particular problem, the learning algorithm will discover this, and allow simulated annealing to control the reproduction process.

Appendix A gives the mathematical form of each of the operators that we use. A basic operator employed in most traditional GA's is known as *n*-point crossover. This operator selects a portion of the gene string from each of two (or more) parent pulse shapes, and then exchanges this section of the gene string between the two parents. The resulting pair of gene strings are the two new children pulse shapes. We use a two-point crossover, which snips the gene string at two random locations and exchanges the genetic information of the two parents between these two locations in order to produce two children. Average crossover also selects two parent gene strings, but rather than exchange genetic information between them, it averages the values of all the genes from the two parents to produce a single child. One important difference between average crossover and two-point crossover is that average crossover can introduce new gene values that were not present in either parent, while two-point crossover simply exchanges values between the two parents.

Another traditional operator that we employ is mutation. This creates a single child from a single parent by randomly reassigning the values of a group of randomly selected genes. Creep, an operator similar to mutation, reassigns values for selected genes incrementally, adjusting the previous values by a small but random amount. Like average crossover, both creep and mutation can introduce new gene values into the population.

Our nontraditional operators only act on the phase genes of the pulses, leaving the amplitudes fixed. One of the nontraditional operators we use is smoothing. The smoothing operator creates a new pulse from a single parent by performing a three-point windowed average over the phase values in the gene string. This operator works very well for problems that require smooth phase profiles across the bandwidth, and it also aids in the interpretation of the results because it produces pulses that are not plagued as much by the entropically driven variations in gene values that sometimes arise from the GA. The action of smoothing as seen in the time domain is to shorten the pulse and reduce structure at long time.

Time-domain crossover is a variation of two-point crossover that first transforms the gene string into a time domain representation of the pulse by performing an inverse fast Fourier transform (IFFT). It then performs a standard two-point crossover on the time domain pulse representation and transforms the pulse back to the frequency domain via a FFT. This operator is useful for problems that involve time domain correlations in the pulse. High-order processes that depend sensitively on $I(t)$ are examples of such problems, and we have shown that the time domain crossover operator performs well in these situations.

Polynomial-phase mutation produces children by replacing a portion of a gene string with a polynomial phase function with a small degree of random variation. The resulting phase profile resembles a polynomial curve over a section of the spectrum. This operator and smoothing work well in conjunction to produce pulses with smooth polynomial phase, which have simpler interpretations in a time-frequency (i.e., Wigner or Husimi) representation [17].

C. Adaptive operators

The adaptive algorithm determines how to best solve a problem by evaluating ''operator fitnesses.'' Like the individual pulse shapes, each of the operators in the pool is evaluated to form a basis for operator selection; each operator is chosen to produce new pulse shapes with a probability proportional to its own fitness. The operator fitnesses are controlled by compiling an operator geneology to keep track of the operators responsible for creating each individual, and assigning a ''credit'' anytime an operator produces a very fit new pulse shape. Thus, operators that produce good pulses are given the opportunity to produce more children. Specifically, credit is assigned when either (1) an individual pulse shape in the current generation is more fit than the best pulse shape of the previous generation, or (2) an individual was an ancestor of a pulse shape that is more fit than the best pulse shape of the previous generation. Passing credit back more than one generation is important, since some operators tend to act in concert. For example, mutation may change genes in ways that are not beneficial until combined with certain other genes in the gene string. By combining the changes made by mutation, two-point crossover may be able to produce fitter children. Passing the credit back a generation or two insures that the mutation operator is also rewarded for its contribution.

We begin our algorithm by assigning each operator an initial normalized fitness, or weighting. The initial weightings are determined by various methods, including empirically (from both experiments and simulations) or through prior knowledge of typical algorithm performances. After the first three generations, the operator fitnesses are allowed to evolve. At this point, the weight for each operator has two parts: a base weight (the value of the operator's fitness during the previous generation) and an adaptive weight (the operator's fraction of the total credit assigned to all individuals during the previous three generations). After each subse-

quent generation, each operator's new fitness is a weighted sum of its current base weight (85%) and its current adaptive weight (15%). Adaptive weighting allows the operators that produce better children to increase their operator fitness. This serves two functions. First, this process speeds up the convergence of the algorithm, since the operators that are not producing better children, and therefore not helping the evolution, are prevented from dominating the reproduction process. Second, the fitnesses of the different operators can yield insight into the dynamics of the learning algorithm and also into the physical system itself by monitoring each operator's fitness as a function of the generation. Possible control mechanisms can be tested by introducing new physically motivated operators and evaluating their success. However, the reproductive process is not required to ''know'' about the particular goal for the problem. The success of the algorithm relies on the fact that the adaptive pool of operators searches vast regions of phase space efficiently, finding successful individuals without any prior knowledge.

The full power of the learning algorithm is best put to use in problems where the experimental knobs are all coupled—when the different degrees of freedom are not independent of each other. In our experiments, the phases and amplitudes of the individual colors are coupled by the system Hamiltonian. In a completely decoupled basis, the problem is reduced to a series of simple one-dimensional searches for each of the genes. However, one does not know what this basis is in general. In a coupled basis, crossover has been demonstrated to be a very valuable operator in selecting new pulse shapes that out perform their parents.

IV. EXPERIMENTS

A. Preliminary test of learning feedback: Second harmonic generation in BBO

Many of the characteristics of adaptive learning are demonstrated by the simple control experiment of second-harmonic generation (SHG). Feedback experiments using SHG have previously been carried out with the goal of targeted pulse compression or shaping [18,19]. Our primary goal was to investigate the dynamics of our algorithm and the learning process in a well-characterized and well-studied system. Frequency doubling in a noncentrosymmetric crystal with a large $\chi^{(2)}$ provided us with this opportunity. Even though the interaction of the light field with this system can be described classically, this experiment illustrates features that are relevant to all the experiments described in this paper. In addition we are able to simulate the experimental feedback signal, which allows us to compare learning algorithms on the model with experiment.

In the low-intensity regime, the interaction of the laser pulses with the crystal can be described by a nonlinear polarization that is proportional to the square of the input light field:

$$P_{NL}(2\omega)=\chi^{(2)}E(\omega)^2. \tag{1}$$

This nonlinear polarization acts as a source or driving term in the wave equation for a field at 2ω. The experimental feedback signal is the integrated second-harmonic intensity:

$$F_{\text{signal}}=\int dtE_{2\omega}^2(t)\propto\int dtE_{\omega}^4(t). \tag{2}$$

If the input field strength is not too large, this description of the interaction gives accurate predictions for the second-harmonic generation without including other nonlinear effects. For all of the frequency doubling experiments and simulations, the amplitude of each frequency component in the pulse is kept fixed. Only the phases may vary. The laser pulse energy is therefore constant, and the algorithm determines how to distribute this energy in time.

The optimal pulse shapes are best viewed as Husimi distributions. The Husimi distribution, $Q(t,\omega)$ is calculated from the measured field $E(\omega)$ in the frequency domain:

$$Q(t,\nu)=\int\int dt'd\nu'S(t',\nu')e^{-(\nu-\nu')^2-(t-t')^2}, \tag{3}$$

$$S(t,\nu)=\int E(\nu+\nu')E^*(\nu-\nu')e^{2i\nu't}d\nu'. \tag{4}$$

$S(t,\nu)$ is the Wigner function whose marginals represent the power spectrum $P(\nu)$ and the temporal intensity $I(t)$ of the laser pulse:

$$\int d\nu'S(t,\nu')=I(t), \tag{5}$$

$$\int dt'S(t',\nu)=P(\nu). \tag{6}$$

Husimi distributions are generated using the values of the phase and amplitude that the pulse shaper programs onto each individual pulse shape. We use spectral interferometry on a limited number of pulse shapes to verify the correspondence between the phase and amplitude profile of the pulse and its representation on our pulse shaper. Since each convergence run of the algorithm has the potential to provide a vast amount of information regarding the problem under study, we monitor not only the optimal pulse shape solution, but also compare this solution to other competing solutions from individual generations throughout the run.

Figure 3 shows the Husimi distributions for pulses optimized to either maximize or minimize frequency doubling in β-barium borate (BBO). The results of both simulations and experiments are shown for comparison. Comparison of panels *a* and *c* reveals that experiment and simulation arrive at the same result for maximizing SHG, except for a small amount of quadratic dispersion (chirp) evident in the experimental result that is within our measurement resolution of the laser pulse.

When the algorithm minimizes the SHG, solutions from both the simulation and experiment contain structure in $I(t)$. We initially expected the solutions for the spectral phase $\phi(\omega)$ would contain only the lowest nontrivial order $[\phi(\omega)=k\omega^2]$. Given the AOM's constraint of a maximum allowed phase change between adjacent frequencies in the light pulse, quadratic phase is the most efficient single-order phase variation, since it allows for the greatest amount of total phase variation across the spectrum. However, the al-

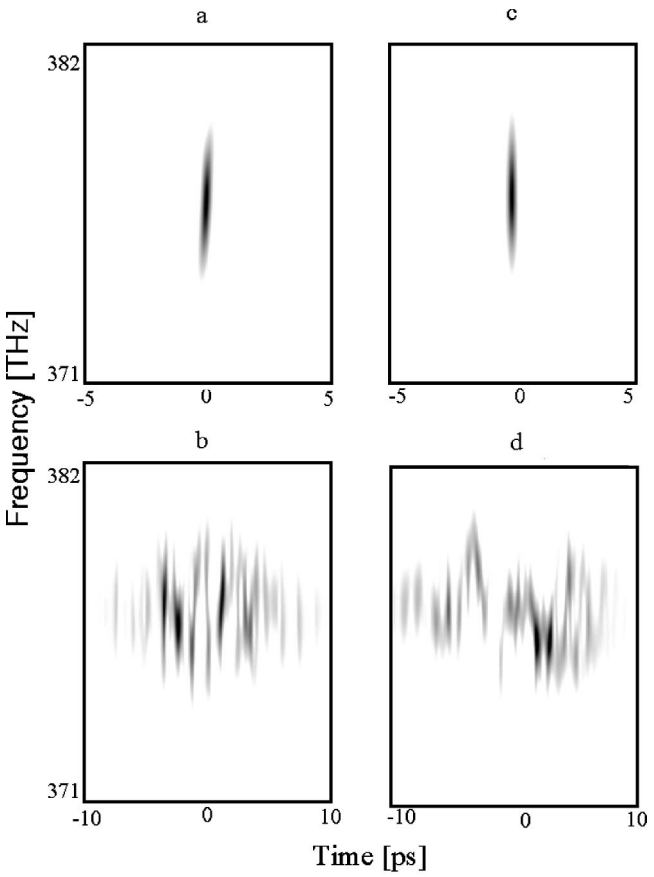

FIG. 3. Husimi distributions of the optimal pulse shapes for SHG in BBO. Panels *a* and *b* are experimental results for maximization and minimization of SHG, respectively. Panels *c* and *d* are the optimal pulse shapes generated using a simulation modeling the SHG process. The value of the Husimi function is indicated by the darkness of the shading.

gorithm finds that a single order of phase is not the most efficient way to minimize $I(t)$ [20]. We evaluated pulses that were simply chirped in time by programming them with the maximum amount of quadratic-only phase allowed by the resolution of our pulse shaper, and found that they did not perform as well as the solutions found by the learning algorithm (see Fig. 3).

Simulations provide rapid testing of the performance of many possible operators. For instance, Fig. 4 shows the best fitness as a function of generation for three different runs of the SHG simulation, both with and without the smoothing operator. The addition of the smoothing operator allows the algorithm to achieve higher fitness more rapidly and converge sooner. In the absence of noise, the best fitness increases monotonically as a function of generation, as guaranteed by elitism.

When the intensity of the light increases, our simple model is no longer adequate to describe the doubling process. Figure 5 shows the changing optimal pulse shape for maximization of SHG as the energy of the input pulse is increased. The optimal pulse in the high-energy solutions acquires large third- and fourth-order dispersion. The shaped pulse spectrum at high intensities shows significant self-

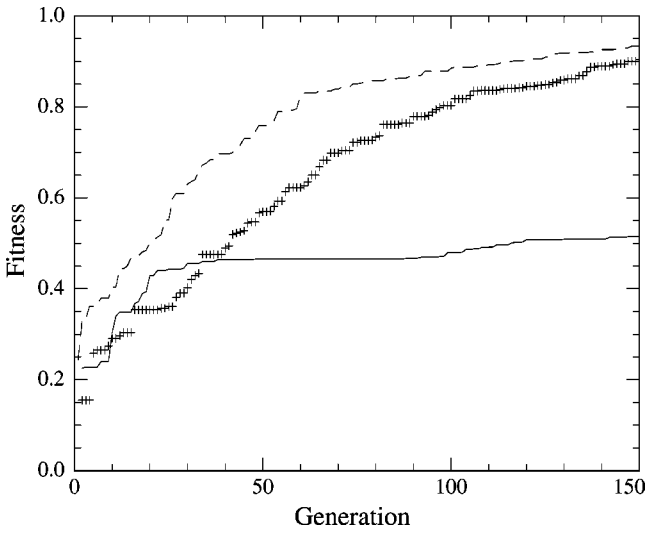

FIG. 4. The fitness of the best individual is plotted as a function of generation for a simulation of SHG maximization. The upper two curves, the dashed and plus lines, compare two runs of the learning algorithm using all the same operators (including *smoothing*), but starting with different random initial populations. The solid line is a third run without the *smoothing* operator.

phase modulation (SPM), whereas in the low-intensity limit there is no evidence of SPM. Simulations are also consistent with SPM in the crystal, which contributes to variations in the solutions as the intensity is increased [21]. At higher pulse energies, SPM is no longer negligible. Evidently, SPM distorts the phase matching for the SHG process, so that a transform limited input pulse is no longer optimal for maximum SHG.

The interplay of multiple operators during the algorithm can yield further insight into the learning process. Figure 6

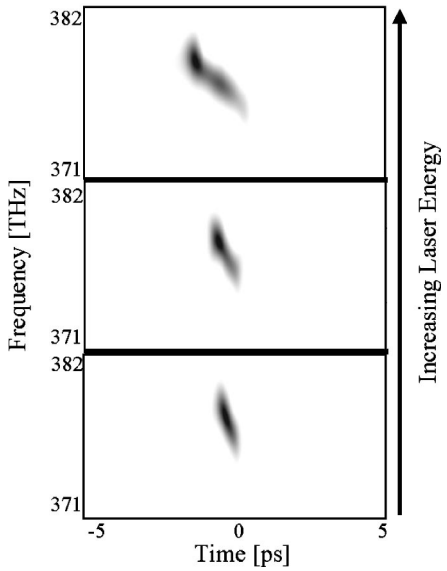

FIG. 5. Husimi plots of the optimal pulse shapes for SHG maximization as the laser energy is increased. At higher input energies (upper panels), the incident pulse contains higher orders of dispersion that broaden the pulse in time.

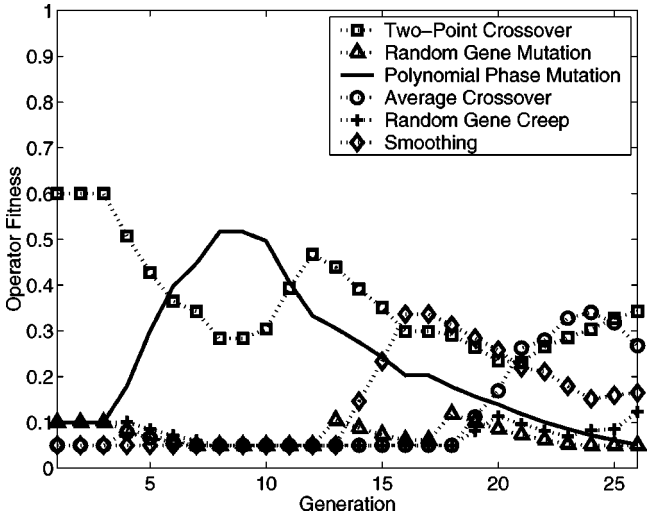

FIG. 6. The fitness for multiple operators plotted as a function of generation for a single run of the learning algorithm while maximizing SHG.

shows the operator fitness as a function of generation for several of our common operators during the frequency doubling experiment. The operators are initialized in a traditional GA configuration, with two-point crossover dominant. For the first few generations, the operators create children in proportion to their initially assigned fitnesses, but after the third generation, their fitnesses are allowed to freely change in accordance with the procedure described earlier. As Fig. 6 demonstrates, the algorithm finds that two-point crossover and simple mutation are not always the best operators, and at different points during the evolution, different combinations of operators become optimal for producing the best children. Polynomial phase mutation, smoothing, and average crossover each produce very fit children at different stages of the run.

This example shows that operators cannot be evaluated in isolation, because they affect each other. For example, smoothing is more important when other operators tend to introduce unnecessary phase variations across the pulse. Also, the performance of the operators cannot be evaluated instantaneously, but must be evaluated over the course of several generations. An operator that is not performing well at one point during the run may become more useful later on. Since some operators that perform poorly at the beginning of the algorithm often perform very well toward the end (e.g., average crossover), their fitness is not allowed to fall below some minimum value (5%). This lower bound ensures that every operator always has some chance of being used during reproduction. Finally, the performance of each operator depends on the problem. Performance of a given operator can help determine whether its action on an individual is physically relevant.

The fitness function assigns each individual pulse shape a single-valued number, reflecting that individual's ability to achieve the goal. Since an individual's fitness is used in parent selection (see Appendix B for details), its determination is an important step in the performance of the algorithm. For the frequency doubling experiment, the fitness assigned to each individual was simply the integrated blue light intensity as measured by a photodiode in a regime where the response of the diode was linear. The frequency doubling experiment, therefore, provides a clear testing ground for the learning algorithm. In other experiments, it is not always so clear how to assign a fitness to each individual, given the nature of the measurement to evaluate the success of each pulse.

B. Controlling dissociative ionization in diatomic sodium

We next explore nonlinear control mechanisms for ionization of diatomic sodium. This experiment provides further opportunities to understand the learning algorithm. However, unlike second-harmonic generation, which can be described classically, this is strictly a quantum system. Here, the adaptive algorithm and pulse shaper must control higher-order nonlinearities. The multiphoton ionization of this system was previously studied using low-energy laser pulses with a single photon resonance enhancement [22]. Our experiments use lower-energy laser photons that are below this resonance.

The shaped pulses were focused into a molecular beam of sodium, causing the molecules to undergo multiphoton ionization. A time-of-flight mass spectrometer allowed identification of molecules that dissociatively ionized and those that did not. The fitness function was a normalized ratio of the ion yield for the two channels. The learning algorithm then worked to optimize either dissociative or nondissociative ionization. As in the doubling experiment, we restricted the algorithm to control only the phases of the colors, with the amplitudes fixed. The algorithm was able to find pulse shapes that could maximize either channel. In the case of maximizing the nondissociative channel, the optimal pulse yielded 88% nondissociative ionization. When we optimized the other channel, we found 73% dissociative ionization.

Figure 7 shows the Husimi distributions for pulses optimized to either nondissociatively or dissociatively ionize the sodium molecules. In addition, the ion yield as a function of the laser energy for an unshaped laser pulse is plotted for both of the channels. The solutions resemble the optimal pulse shapes for the second-harmonic generation experiment (see Fig. 3). For the dissociative channel, the pulse shape is similar to the short-pulse, high-intensity solution of SHG maximization, while for the nondissociative channel, the pulse shape is similar to the long-pulse, low-intensity solution of SHG minimization. These results are consistent with the fact that the two channels in log-log plot have different slopes, and that the branching ratio is a function of intensity.

The sodium experiment demonstrates the importance of the choice of basis for encoding pulse shapes. The learning algorithm incorporates the time-domain crossover operator, which allows it to choose the basis best suited to the problem. Figure 8 shows the operator fitnesses as a function of generation when optimizing the nondissociative channel. There are five operators—four in the usual frequency basis, and the time-domain crossover operator in the time basis. As Fig. 8 shows, the time-domain crossover operator increases its fitness at the expense of the operators working in the frequency basis. Correlations in the time domain are an important control parameter for this problem, as expected.

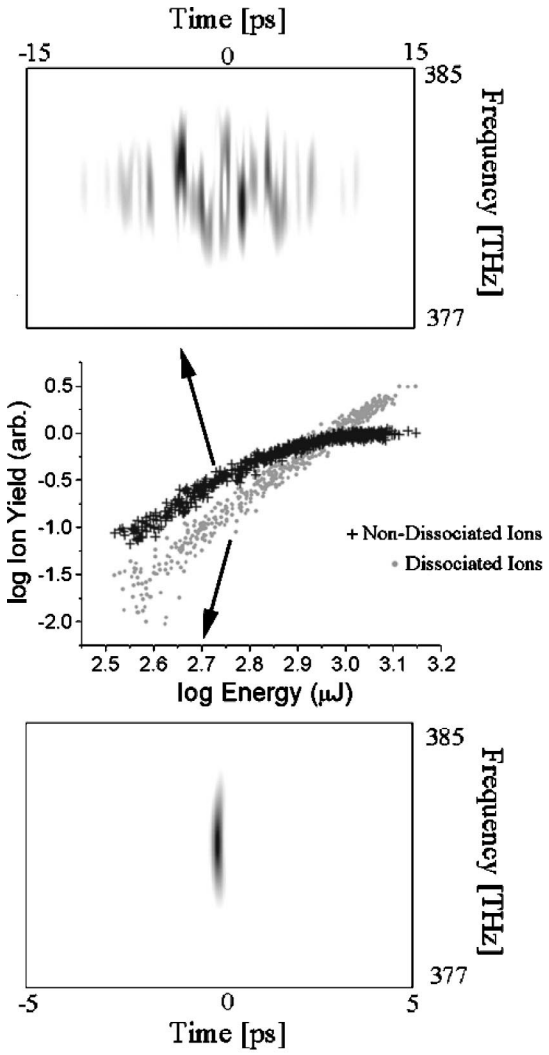

FIG. 7. Husimi distributions of the optimal pulse shape for controlling sodium ionization. The upper plot is for maximizing the nondissociative yield, while the lower plot is for the dissociative yield. In between is a $\log_{10}$-$\log_{10}$ plot of the ion yield into each of the two channels as a function of the energy of an unshaped laser pulse.

Another possible control mechanism involves the parity of the phase profile of the pulse: Is the phase as a function of frequency an even function, an odd function, or neither about the central frequency? Parity control in nonlinear atomic absorption was previously demonstrated by Meshulach and Silberberg [4]. The amount and sign of chirp on the pulse is another possible way to control the population dynamics [5]. We investigated both possibilities using our pulse shaper and feedback, but saw no conclusive dependence on the dissociation fraction with either method. The adaptive pool of operators performs a more effective search of the phase space.

C. Controlling molecular liquids

Molecular liquids pose a greater challenge for learning control, because of rapid relaxation and inhomogeneous broadening. Our initial goal was to control molecular vibrations in liquids through impulsive stimulated Raman scattering. Impulsive scattering occurs when the laser pulse is shorter than the vibrational period of the molecule. In the frequency domain, this means that the bandwidth of the laser is broad compared to the vibrational energy spacing of the mode in question. The result is that a stimulated Stokes wave can be seeded with light that is already present in the laser and does not have to build up from noise, thereby making the process much more efficient than the nonimpulsive case. Shaped laser pulses should allow selective control over excitation of Raman modes since the pulse shaper can modulate the spectrum of $E^2(\omega)$, the driving term in Raman excitation [23]. In the time domain, this corresponds to resonantly driving some modes but not others.

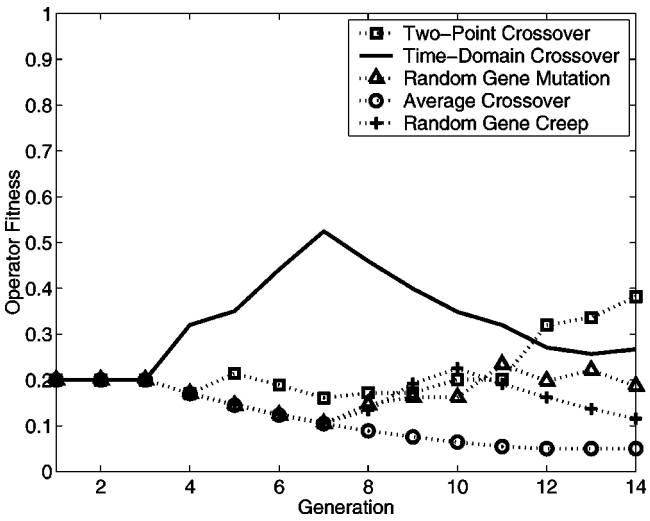

FIG. 8. Operator fitness as a function of generation for multiple operators for optimizing the nondissociative ionization channel of sodium.

1. Controlling SPM in liquids

Impulsive scattering in a multimode molecular liquid was studied in CCl_4 because it has several low frequency modes with relatively high cross sections. We discovered, however, that it also has a large polarizability, and therefore, most of the light that was scattered near the laser bandwidth in the forward direction was a result of SPM. We found that we had a significant degree of control over the spectrum of the forward scattered light, and so as an initial demonstration of the capabilities of the apparatus, we studied the nonlinear frequency shift of intense light propagating in CCl_4. Early results of this investigation were previously published [24]. Here, we describe the learning process and analyze the solutions in more detail.

Feedback goals for SPM are based upon small features that are barely visible in the spectra of the forward scattered radiation after unshaped pulses illuminate the sample. These modulations are typical spectral features for pulses that have undergone SPM [25]. The learning algorithm is able to control their frequency and phase by altering the shape of the driving pulse. Only phase modulation is used, so that the pulse energy is fixed. Figure 9 shows the spectra of four different pulses after propagating through the CCl_4 sample. The first panel shows the spectrum for an unshaped pulse, and the following three panels show spectra for pulses that

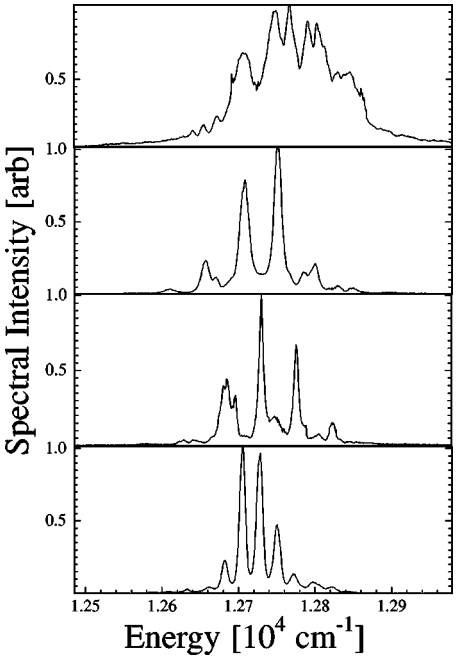

FIG. 9. Power spectra for pulses propagating through 1 cm of CCl_4. The top panel shows the power spectrum for an unshaped laser pulse. The following three panels show spectra for pulses shaped to control (and enhance) the spectral modulations. (From Ref. [24], reprinted by permission.)

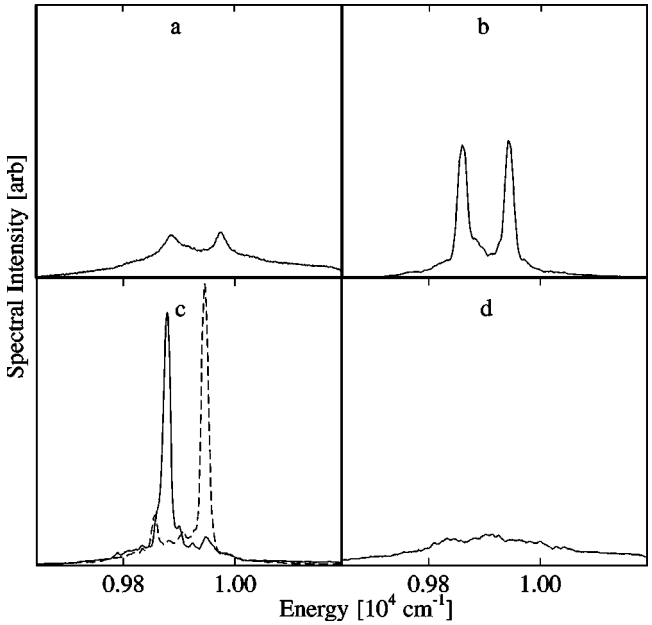

FIG. 10. Control of Raman scattering in methanol. Panel *a* shows the forward scattered spectrum for an incident unshaped laser pulse. Panel *b* shows the spectrum after the learning algorithm optimized excitation of both modes while minimizing peak broadening due to other nonlinear effects. Panel *c* shows spectra for optimization of each mode independently. Panel *d* shows the spectrum for a pulse that minimized Raman scattering from both modes. (From Ref. [24], reprinted by permission.)

are shaped to control the spectral modulations.

Model calculations can determine whether SPM is responsible for the observed spectra. The simplest description of SPM, which doesn't include spatial effects such as self focusing, characterizes the nonlinear interaction between the laser and the medium through a intensity-dependent index of refraction:

$$n(t)=n_0+n_2I(t), \tag{7}$$

where n_0 is the field free index, I is the instantaneous laser intensity, and n_2 is an empirically determined coefficient. The calculated power spectra for laser pulses that have acquired a phase proportional to their instantaneous intensity show intensity modulations with the same dependence on pulse shape that we found in the experiment (see Fig. 9).

2. Controlling vibrations in multimode molecular liquids

The learning algorithm can also control the interaction between the driving laser pulse and the vibrational modes of a multimode molecule without making use of impulsive scattering. In order to avoid confusion between Stokes light and light generated by SPM alone, we chose a molecule with a much larger Stokes shift, since there is much less light generated through SPM further from the central laser frequency. Methanol (CH_3OH) is ideal because it has two closely spaced modes with large Stokes shifts and large cross sections. Forward scattered radiation is the feedback for the algorithm. There is no backwards scattered Stokes radiation because of the short duration of the shaped pump pulse ($\sim$1 ps). The forward-backward symmetry of the scattering is broken for a short pump pulse because the backward traveling Stokes wave passes through the pump wave before any appreciable buildup [26].

The time scales for the interaction between the molecules and the laser pulse are set by the vibrational period of the active modes and their coherence time. Stimulated scattering with pulses that are longer than the coherence time reaches a steady state and exhibits a strong dependence on pulse duration because it is a stimulated process: The more photons that interact with the molecules within the coherence time, the more likely the molecule will be stimulated to absorb a laser photon and emit a Stokes photon. Scattering with pulses that are shorter than the coherence time but longer than the vibrational period (transient Raman scattering) exhibits little dependence on the duration of the laser pulse [27,28]. Scattering with pulses that are shorter than the vibrational period (impulsive scattering) results in very efficient stimulated scattering as discussed above [29,30].

With an unshaped laser pulse focused into 10 cm of methanol, the spectrum shown in Fig. 10(a) is obtained. The two small peaks in the spectrum correspond to Stokes light for $\delta\nu=1$ for the symmetric and asymmetric C-H stretch modes. The lens focal length is 40 cm. The first feedback goal is to maximize the contrast between the two Stokes peaks and the background light resulting from SPM. The forward scattered spectrum in the spectral range of the Stokes radiation is collected for each laser pulse. The number of Stokes photons at a particular frequency is a measure of the number of molecules excited in that particular mode;

however, since SPM is present and the bandwidth of the shaped laser pulses is large, the forward scattered spectrum also contains some misleading information. The feedback function must filter this out. Different fitness functions work best, depending on which peak(s)are optimized. A typical fitness function is:

$$\sum_{\omega_r<\omega_i<\omega_b} \frac{NC(\omega_i)}{\omega_b-\omega_r} - \sum_{\omega_i>\omega_b,\omega_i<\omega_r} \frac{C(\omega_i)}{\Delta\omega-(\omega_b-\omega_r)}. \quad (8)$$

Here, $C(\omega_i)$ is the number of spectrometer counts at ω_i, $\Delta\omega$ is the bandwidth of the spectrometer, ω_r is the low-frequency limit for the desired peak, ω_b is the high-frequency limit for the desired peak and N is an empirically determined integer. We set the values of ω_r and ω_b by narrowing the bandwidth of shaped laser pulse and measuring the width of the Stokes peaks in the forward scattered spectrum. We find that $N=2$ and $N=3$ work well. A pulse solution that optimizes the contrast between the two Stokes peaks and the background is shown in Fig. 10(b).

The next goal is to generate spectra with each peak separately. These spectra, shown in Fig. 10(c), correspond to exciting symmetric or antisymmetric modes alone. The Stokes shift for these modes is large compared to the bandwidth of the driving laser pulse. This is equivalent to saying that the Raman excitation is nonimpulsive, and therefore, one cannot seed the Stokes radiation directly with the laser light. Our final feedback goal is to eliminate all forward scattered light at either of the two Stokes frequencies, with the resulting spectrum shown in Fig. 10(d).

3. Using the adaptive algorithm to investigate possible control mechanisms for SRS in methanol

The Stokes shift for the C-H stretch is almost 3000 cm^{-1} and the laser bandwidth is roughly 100 cm^{-1}, so the scattering is definitely nonimpulsive. Another possible mechanism that could account for our ability to selectively excite the symmetric or asymmetric stretch mode of methanol is a coupling between the electronic polarizability of the atoms and the vibrational modes. The results with CCl_4 have shown that the light generated from SPM of the pump beam is very sensitive to the input pulse shape. A large contribution to SPM, particularly for femtosecond pulses, is the atomic polarizability [31]. Perhaps the atomic polarizability generates SPM to seed one of the two Raman modes but not the other.

This hypothesis was tested by replacing the methanol with a mixture of benzene (C_6H_6) and deuterated benzene (C_6D_6). Similar control experiments were attempted, except now the two modes of vibration were in two different molecules. The ring breathing mode of benzene ($\nu=992$ cm^{-1}) has a large Raman cross section making excitation easy. Deuterated benzene has a frequency of $\nu_D=945$ cm^{-1}, which is shifted by 47 cm^{-1}, similar to the mode splitting in methanol. Initially, an unshaped laser pulse was focused into the experimental cell with pure C_6H_6, and we measured no forward scattered Stokes light. We then used the learning algorithm to find a shaped pulse that generates the forward scattered Stokes radiation shown in Fig. 11 (top panel, left curve). The deuterated benzene (C_6D_6) generates the spectrum shown in Fig. 11 (top panel, right curve), demonstrating the expected shift of the mode frequency. Finally, a 50/50 mixture of C_6H_6 and C_6D_6 is placed in the cell and we ask the algorithm to selectively drive each of the two modes. Figure 11(bottom panel) shows the learning algorithm can select the C_6H_6 mode but not the C_6D_6 mode. This demonstration of a lack of control is consistent with the idea that the mode selection is an intramolecular effect that relies on coupling between the two modes inside each molecule, rather than seeding of one of the modes with light from SPM.

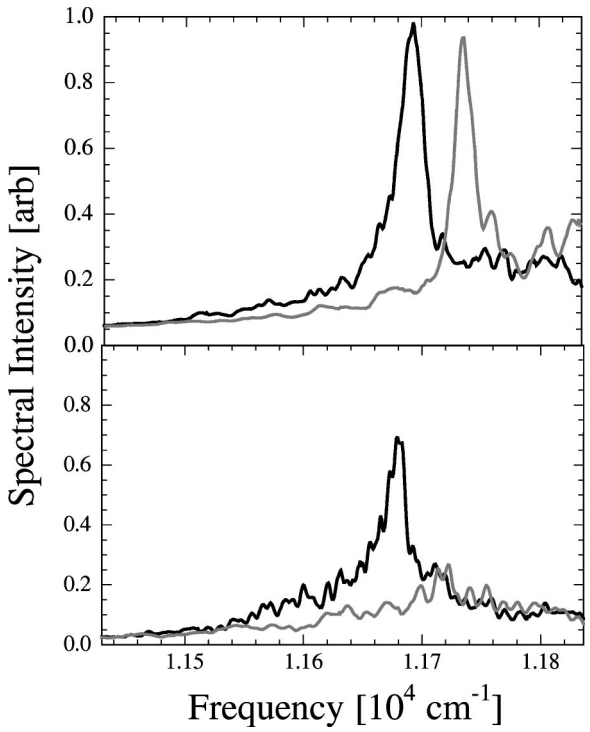

FIG. 11. Stimulated Raman scattering in C_6H_6 and C_6D_6. Top panel shows spectra for C_6H_6 (left curve) and C_6D_6 (right curve) separately after optimization of the pulse shape to excite the breathing mode of each molecule. Bottom panel shows the results after using the learning algorithm to excite each molecule separately in a 50-50 mixture of the two.

Another experiment supports this conclusion: Experiments conducted in CO_2 gas show that light generated by SPM more than a few hundred cm^{-1} away from the laser frequency is extremely noisy and not reproducible [32]. The reproducibility of SPM spectra increases nearer the frequency of the driving laser. Figure 9 shows that SPM produces stable spectra very near the laser frequency. However, far from the laser at the frequency of the Stokes light from the C-H stretch mode, the light produced by SPM would be too noisy to reproducibly seed one of the two Raman modes but not the other.

Another possible control mechanism is suggested by analyzing the optimal pulse shape solutions for exciting each of the two modes. Figure 12 shows the Husimi distribution for pulses that were optimized for excitation of the asymmetric stretch mode in methanol, while Fig. 13 shows the Husimi

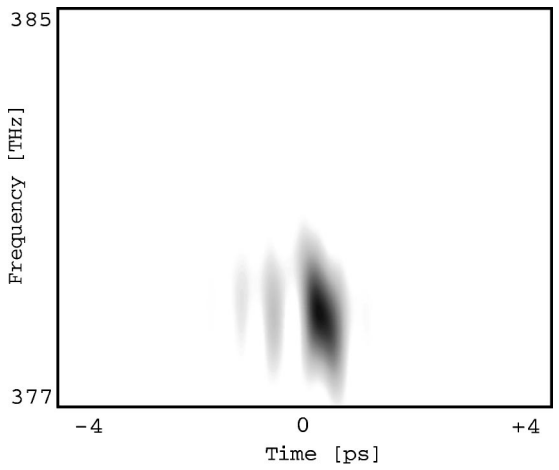

FIG. 12. Husimi plot of the optimal pulse shape to excite the asymmetric stretch in methanol.

distribution for pulses optimized for excitation of the symmetric stretch mode. The structure of the optimal pulse shape for the symmetric stretch mode suggests a ''quasi-impulsive'' model, where the frequency separation of the two subpulses is exactly the beat frequency between the symmetric and asymmetric modes. The term ''quasi-impulsive'' is used, since although the laser bandwidth is narrow compared to the Stokes shift of each mode, it is wide in comparison to the spacing between the modes. This is equivalent to saying that in the time domain, the laser pulse is long compared to the vibrational period of the modes, but short compared to the beat note between them. The beat note period is 285 fs, while the time duration of the unshaped laser pulse is 150 fs. Therefore, energy could be transferred between the two modes by engineering temporal structure in the driving pulse at the coupling frequency between the two modes. Once an initial vibrational population is established in some combination of the two modes, the population could be redistributed by the shaped pulse through an impulsive coupling of the two levels.

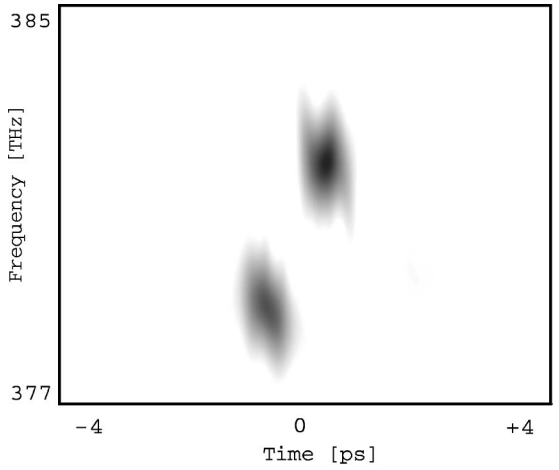

FIG. 13. Husimi plot of the optimal pulse shape to excite the symmetric stretch in methanol.

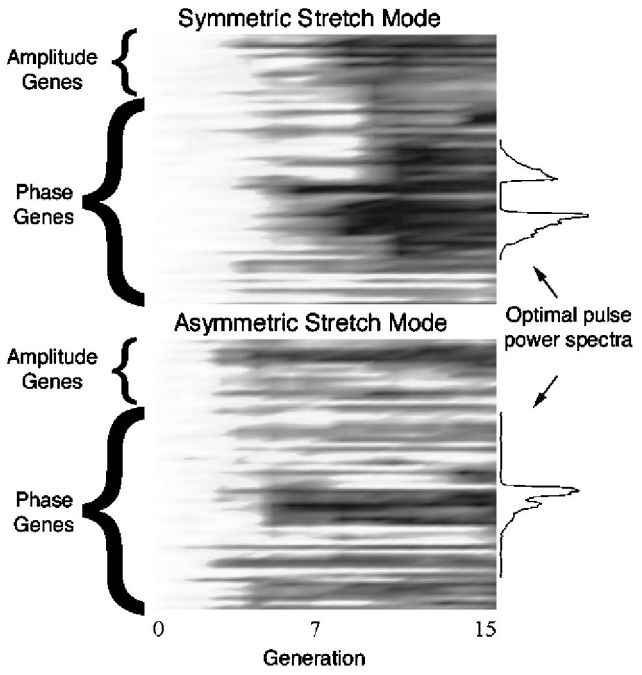

FIG. 14. Genetic variation as a function of generation. Data is shown for two separate runs of the learning algorithm. Top panel shows the genetic variation for optimization of the symmetric stretch mode, and the bottom panel for optimization of the asymmetric stretch mode. The vertical axis represents the gene number. For reference, the power spectra are overlayed to the right of the phase genes. Light shading represents a large degree of variation among the individuals, while dark shading represents low variation.

General trends in an entire population can provide valuable information, since looking at a single individual, even if it is the very best pulse shape of the group, does not give information about which features are necessary and which are merely sufficient. One cannot tell whether a feature in the pulse shape plays some physical role in the process under investigation, or whether the algorithm simply did not remove the feature since its presence did not degrade the fitness. We test this by repeating a convergence sequence of the learning algorithm with different random initial populations. If the best solution has similar structure multiple times, it is likely that the structure is physically necessary.

Statistical variations among gene values of individuals in a population also reveals which genes are important for a given problem and which are not. Figure 14 shows the genetic variation as a function of generation for a run of the algorithm during the methanol experiment. Light shading represents a large degree of variation among individuals for the value of a given gene, while dark shading represents low variation. The variation is the normalized sum of the absolute values of the differences between all of the genes' values in a given location on the gene string:

$$\sum_{i,j>i}^{N} |g_i - g_j|, \tag{9}$$

where $g_{i,j}$ is the value of gene g for the ith, jth individual. Since the genes are randomly initialized, all the genes begin

with a light shading. As the algorithm converges, all gene values become more similar through mating. The plots verify the intuitive idea that near convergence, frequency components whose amplitudes are large have smaller variation in their programmed phase values than frequency components whose amplitudes are zero. The power spectra shown at right match with the darker regions (smaller variation) in the plots.

V. CONCLUSIONS

We have demonstrated control over a variety of systems using an adaptive learning algorithm. The algorithm uses a variety of searching methods and adapts itself in order to arrive at an optimal solution. This learning technique is general and can be applied to other systems since the interaction does not require specific resonances and no prior knowledge of the system Hamiltonian is required. The adaptive approach provides information about the physical system through examination of the solutions, the operator dynamics, and the choice of basis. Future goals include controlling bond excitation to drive reactions in bimolecular solutions.

ACKNOWLEDGMENTS

The authors would like to acknowledge very helpful and informative discussions with Marcus Motzkus, Ronnie Kosloff, Misha Ivanov, and Robert Levis, as well as Daniel Morris for technical assistance. This work was supported by the National Science Foundation under Grant No. 9987916.

APPENDIX A: DEFINITIONS OF OPERATORS

We have r_i=a random number in [0,1], P=parent, C=child, Φ=phase, A=amplitude. All phases are referenced to adjacent genes to maintain continuity. We use multiple forms for some of the operators.

Two-point crossover:

$$P_1=[\Phi_{p1}(\omega_i),A_{p1}(\omega_i)],\quad P_2=[\Phi_{p2}(\omega_i),A_{p2}(\omega_i)]$$

$$C_1=\begin{cases}[\Phi_{p2}(\omega_i),A_{p2}(\omega_i)] & \text{if } j<i<k\\ [\Phi_{p1}(\omega_i),A_{p1}(\omega_i)], & \text{all other i,}\end{cases}$$

$$C_2=\begin{cases}[\Phi_{p1}(\omega_i),A_{p1}(\omega_i)] & \text{if } j<i<k\\ [\Phi_{p2}(\omega_i),A_{p2}(\omega_i)], & \text{all other i.}\end{cases}$$

Average crossover:

$$P_1=[\Phi_{p1}(\omega_i),A_{p1}(\omega_i)],\quad P_2=[\Phi_{p2}(\omega_i),A_{p2}(\omega_i)]$$

$$C=\begin{cases}\left[\dfrac{\Phi_{p1}(\omega_i)+\Phi_{p2}(\omega_i)}{2},\dfrac{A_{p1}(\omega_i)+A_{p2}(\omega_i)}{2}\right] & \text{if } j<i<k\\ [\Phi_{p_1}(\omega_i),A_{p_1}(\omega_i)], & \text{all other i.}\end{cases}$$

Mutation:

$$P=[\Phi_p(\omega_i),A_p(\omega_i)],$$

$$C=\begin{cases}[\pm 2\pi r_i,Ap(\omega_i)] & \text{if } j<i<k\\ [\Phi_p(\omega_i),A_p(\omega_i)], & \text{all other i.}\end{cases}$$

Polynomial phase mutation:

$$P=[\Phi_p(\omega_i),A_p(\omega_i)],$$

$$C=\begin{cases}[\pm\omega_i^n,A_p(\omega_i)] & \text{if } j<i \text{ or } i<k\\ [\Phi_p(\omega_i),A_p(\omega_i)], & \text{all other i,}\end{cases}$$

where n=an integer in $[0,6]$.

Creep:

$$P=[\Phi_p(\omega_i),A_p(\omega_i)],$$

$$C=\begin{cases}[\Phi_p(\omega_i)\pm 0.25,A_p(\omega_i)\pm\text{one level}] & \text{if } r_i<0.10\\ [\Phi_p(\omega_i),A_p(\omega_i)], & r_i\geqslant 0.10.\end{cases}$$

Smooth:

$$P=[\Phi_p(\omega_i),A_p(\omega_i)],$$

$$C=\left[\frac{\Phi_p(\omega_i)+\Phi_p(\omega_{i+1})+\Phi_p(\omega_{i-1})}{3},A_p(\omega_i)\right].$$

Time-domain crossover:

$$P_1=[\Phi_{p1}(\omega_i),A_{p1}(\omega_i)],\quad P_2=[\Phi_{p2}(\omega_i),A_{p2}(\omega_i)],$$

$$P_1'=\text{IFFT}[\Phi_{p1}(\omega_i),A_{p1}(\omega_i)]\equiv E_1(t_i),$$

$$P_2'=\text{IFFT}[\Phi_{p2}(\omega_i),A_{p2}(\omega_i)]\equiv E_2(t_i),$$

$$C_1'=\begin{cases}[E_1(t_i)] & \text{if } j<i<k\\ [E_2(t_i)], & \text{all other i,}\end{cases}$$

$$C_2'=\begin{cases}[E_2(t_i)] & \text{if } j<i<k\\ [E_1(t_i)], & \text{all other i,}\end{cases}$$

$$C_1=\text{FFT}(C_1'),$$

$$C_2=\text{FFT}(C_2')$$

with amplitudes kept fixed to one.

APPENDIX B: DETAILS OF FITNESS FUNCTION

Each individual is evaluated, and a single-valued fitness is returned to the algorithm. Each individual's fitness is transformed into a scaled fitness used for parent selection during reproduction. The fitness scaling helps to ensure there is an adequate degree of ''selection pressure,'' which is a measure of how much successful pulse shapes are rewarded. Maintaining selection pressure becomes difficult when the range of fitness values decreases as the algorithm converges. Without fitness scaling, the algorithm can stagnate since more fit pulse shapes receive little reward. Specifically, we use a linear scaling technique:

$$(\text{Scaled fitness})=\frac{(\text{Best fitness})-(\text{Unscaled fitness})}{(\text{Average fitness})-(\text{Best fitness})}+2$$

Any scaled fitnesses less than zero are reset to zero. With this scaling method the best pulse shape is selected as a parent twice as often as the average pulse shape.

[1] R. Judson and H. Rabitz, Phys. Rev. Lett. **68**, 1500 (1992).
[2] L. Zhu, V. Kleiman, X. Li, S. Lu, K. Trentelman, and R. J. Gordon, Science **270**, 77 (1995).
[3] A. Assion, T. Baumert, M. Bergt, T. Brixner, B. Kiefer, V. Seyfried, M. Strehle, and G. Gerber, Science **282**, 919 (1998).
[4] D. Meshulach and Y. Silberberg, Nature (London) **396**, 298 (1998).
[5] C. J. Bardeen, V. V. Yakovlev, K. R. Wilson, S. D. Carpenter, P. M. Weber, and W. S. Warren, Chem. Phys. Lett. **280**, 151 (1997).
[6] J. J. Gerdy, M. Dantus, R. M. Bowman, A. H. Zewail, Chem. Phys. Lett. **171**, 1 (1990).
[7] A. P. Heberle, J. J. Baumberg, and K. Khler, Phys. Rev. Lett. **75**, 2598 (1995).
[8] N. H. Bonadeo, J. Erland, D. Gammon, D. Park, D. S. Katzer, and D. G. Steel, Science **282**, 1473 (1998).
[9] A. Haché, Y. Kostoulas, R. Atanasov, J. L. P. Hughes, J. E. Sipe, and H. M. van Driel, Phys. Rev. Lett. **78**, 306 (1997).
[10] *Handbook of Genetic Algorithms*, edited by L. Davis (Van Norstrand Reinhold, New York, 1991).
[11] D. N. Fittinghoff, J. L. Bowie, J. N. Sweester, R. T. Jennings, M. A. Krumbugel, K. W. DeLong, R. Trebino, and I. A. Walmsley, Opt. Lett. **21**, 884 (1996).
[12] J. X. Tull, M. A. Dugan, and W. S. Warren, Adv. Magn. Opt. Reson. **20**, 1 (1990).
[13] T. C. Weinacht, J. Ahn, and P. H. Bucksbaum, Nature (London) **397**, 233 (1999).
[14] Hans-Paul Schwefel, *Evolution and Optimum Seeking* (Wiley, New York, 1995).
[15] T. Hornung, R. Meier, D. Zeidler, K. L. Kompa, D. Proch, and M. Motzkus, Appl. Phys. B: Lasers Opt. **71**, 277 (2000).
[16] D. Adler, in *Proceedings of the 1993 IEEE International Conference on Neural Networks* (SOS Printing, San Diego, 1993).
[17] J. Paye, IEEE J. Quantum Electron. **28**, 2262 (1992).
[18] D. Meshulach, D. Yelin, and Y. Silberberg, J. Opt. Soc. Am. B **15**, 1615 (1998).
[19] T. Baumert, T. Brixner, V. Seyfried, M. Strehle, and G. Gerber, Appl. Phys. B: Lasers Opt. **65**, 779 (1997).
[20] V. S. Malinovsky and J. L. Krause, Phys. Rev. A **63**, 043415 (2001).
[21] E. J. T. Nibbering, M. A. France, B. A. Prade, G. Grillon, C. Le Blanc, and A. Mysryowicz, Opt. Commun. **119**, 479 (1995).
[22] T. Baumert, B. Bhler, R. Thalweiser, and G. Gerber, Phys. Rev. Lett. **64**, 733 (1990).
[23] P. H. Bucksbaum, Nature (London) **396**, 217 (1998).
[24] T. C. Weinacht, J. L. White, and P. H. Bucksbaum, J. Phys. Chem. A **103**, 10166 (1999).
[25] P. Corkum and C. Rolland, IEEE J. Quantum Electron. **25**, 2634 (1989).
[26] Y. R. Shen, *The Principles of Nonlinear Optics* (Wiely, New York, 1984).
[27] R. L. Carman, F. Shimizu, C. S. Wang, and N. Bloembergen, Phys. Rev. A **2**, 60 (1970).
[28] R. L. Carman, M. E. Mack, F. Shimizu, and N. Bloembergen, Phys. Rev. Lett. **23**, 1327 (1969).
[29] G. Korn, O. Duhr, and A. Nazarkin, Phys. Rev. Lett. **81**, 1215 (1998).
[30] A. Nazarkin and G. Korn, Phys. Rev. A **58**, R61 (1998).
[31] R. W. Hellwarth, A. Owyoung, and N. George, Phys. Rev. A **4**, 2342 (1971).
[32] T. C. Weinacht, Ph.D. thesis, University of Michigan, 2000.